THE ASTROPHYSICAL JOURNAL, 454:688–697, 1995 December 1

BROAD Ne VIII λ774 EMISSION FROM THE QUASAR PG 1148+549

FRED HAMANN
Center for Astrophysics and Space Sciences, University of California, San Diego, La Jolla, CA 92093-0111; hamann@cass157.ucsd.edu

JOSEPH C. SHIELDS[1]
Steward Observatory, University of Arizona, Tucson, AZ 85721

AND

GARY J. FERLAND AND KIRK T. KORISTA
Department of Physics and Astronomy, University of Kentucky, Lexington, KY 40506
Received 1995 February 27; accepted 1995 June 12

ABSTRACT

We discuss the probable detection of broad Ne VIII λ774 emission from the $z_e = 0.978$ quasar PG 1148+549, and we use spectral synthesis calculations to study the physical conditions in the line-forming gas. The theoretical predictions and the measured line wavelength both support Ne VIII λ774 as the most likely identification.

Our calculations show that Ne VIII λ774 forms in hotter and more highly ionized gas than previously recognized in the broad emission line region. If the gas is photoionized by a standard active galactic nucleus continuum, the observed Ne VIII equivalent width, the Ne VIII/O VI flux ratio, and the assumption of cloud stability imply ionization parameters $5 \lesssim U \lesssim 30$ and temperatures 5×10^4 K $\lesssim T_e \lesssim 2 \times 10^5$ K. The large Ne VIII equivalent width also suggests that the emitting clouds cover $\gtrsim \frac{1}{3}$ of the continuum source and have a total hydrogen column density $N_H \gtrsim 10^{22}$ cm^{-2}. If the gas is instead collisionally ionized, Ne VIII could reside in stable clouds with equilibrium temperatures near 8×10^5 K. In either case, the Ne VIII–emitting clouds will appear as X-ray "warm absorbers" if they lie along our line of sight to the X-ray continuum source.

Line thermalization can greatly lower some of the line fluxes and alter the line ratios. For example, C IV λ1549 can be thermalized easily, with doublet emission ratios λ1548/λ1550 near unity. However, our calculations indicate that Ne VIII λ774 is *not* thermalized and that its doublet emission ratio should be λ770/λ780 ≈ 2. Future observations of the widely separated Ne VIII doublet would test this prediction and constrain the space and column densities in the Ne VIII emitting region.

Finally, temperatures in the Ne VIII gas may be in the range needed for optically thin models of the UV continuum, i.e., the "big blue bump." However, the diffuse thermal continuum flux from the Ne VIII–emitting region falls well short of the observed continua unless the measured lines are severely suppressed by thermalization at densities $\gtrsim 5 \times 10^{12}$ cm^{-3}. This result supports Kriss's claim that the optically thin blue-bump models have the serious problem of overpredicting the UV metal line fluxes.

Subject headings: galaxies: ISM — line: formation — line: identification — quasars: emission lines — quasars: individual (PG 1148+549) — ultraviolet: galaxies

1. INTRODUCTION

PG 1148+549 ($V = 15.8$ mag) is a radio-quiet QSO, discovered in the Palomar Bright Quasar Survey (Schmidt & Green 1983; Kellermann et al. 1989). Published spectra of this source obtained with the *IUE* satellite show the usual broad emission lines (BELs) in the UV, including Lyα, C IV λ1549, N V λ1240, and O VI λ1034 (Kinney et al. 1991; Lanzetta, Turnshek, & Sandoval 1993). Tytler & Fan (1992) measured an emission redshift of $z_e = 0.978$ from ground-based observations of its C III] λ1909 and Mg II λ2798 line peaks.

The existing *IUE* spectra of PG 1148+549 contain a previously unreported broad emission feature at ~1500 Å (observed) that could be the very high ionization line Ne VIII λ774. This line is the counterpart of the more readily observable C IV, N V, and O VI transitions in the lithium isoelectronic sequence, but Ne VIII λ774 has not yet been clearly identified in any active galactic nucleus (AGN—we consider the class of AGNs to include QSOs and the less luminous Seyfert galaxies). However, recent studies of *Hubble Space Telescope* (*HST*) spectra suggest that Ne VIII emission could be quite common (Cohen et al. 1995; Hamann, Zuo, & Tytler 1995b). We are now pursuing *HST* observations to test the Ne VIII identification and determine the strength and frequency of Ne VIII emission in QSO samples.

In this paper we discuss the *IUE* spectrum of PG 1148+549 and explore the general implications of Ne VIII λ774 emission. There are several reasons why this line deserves special attention.

1. The ionization energy required for Ne VIII, 207 eV, is considerably larger than the energies needed for other well-known ions in the broad emission line region (BELR). For example, C IV, N V, and O VI require energies of only 48, 77, and 114 eV, respectively. Therefore, Ne VIII λ774 would identify a much higher ionization component of the BELR than previously recognized.

2. The ionization implied by Ne VIII is consistent with that of X-ray "warm" (ionized) absorbers measured in many

[1] Hubble Fellow.

nearby AGNs (Netzer 1993; Shields, Ferland, & Peterson 1995; Hamann et al. 1995a; see also § 6.2). The X-ray warm absorbers are characterized by O VII or O VIII absorption edges at ~0.8 keV or by X-ray continuum opacities that vary inversely with the X-ray flux (Halpern 1984; Krolik & Kallman 1984; Netzer 1993; Fiore et al. 1993; Nandra & Pounds 1994). Recently, Shields (1994) and Shields et al. (1995) described how these optically thin, warm absorbers might contribute significantly to the UV emission lines. George, Turner, & Netzer (1995) observationally linked the highly ionized emission and absorption regions via simultaneous detections of soft X-ray O VII–O VIII emission lines and bound-free edges in the AGN NGC 3783. Similarly, Kaastra, Roos, & Mewe (1995) reported the presence of Ne VII–Ne VIII emission lines at ~88 Å in another AGN with X-ray O VII–O VIII absorption, NGC 5548. Mathur et al. (1994) and Mathur (1994) claimed that the highly ionized X-ray absorbers also produce associated ($z_a \approx z_e$) UV absorption lines in at least two QSOs. That connection is supported by measurements of associated Ne VIII λ774 absorption in one $z_e = 2.15$ QSO, UM 675, where the time-variable lines require absorption within 200 pc of the continuum source (Hamann et al. 1995a; Junkkarinen et al. 1995). Searches for broad Ne VIII λ774 emission could test the hypothesis that all of the highly ionized absorbing regions are part of, or related to, the BELR (Shields 1994).

3. Ne VIII λ774 emission might also trace the gas responsible for the UV continuum, i.e., the "big blue bump" (BBB), in AGN spectra. The BBB is generally described as thermal radiation from either an optically thick accretion disk (Malkan & Sargent 1982; Laor & Netzer 1989) or an optically thin region that reprocesses high-energy photons into the optical and near-UV (Antonucci & Barvainis 1988; Ferland, Korista, & Peterson 1990; Ferland & Rees 1988; Barvainis 1993). We will show below that the temperatures and column densities needed for Ne VIII emission (and absorption) might be in the range needed for optically thin models of the BBB, but that the diffuse continuum flux from the Ne VIII gas is too weak to explain the BBBs unless the lines are severely suppressed by thermalization at high densities.

4. Finally, Ne VIII λ774 is actually a widely separated doublet, whose components at ~770 Å and ~780 Å are ~3850 km s^{-1} apart and potentially resolvable in AGN spectra. Observations of this doublet ratio would constrain the amount of line thermalization and thus the space and column densities in the hot BELR.

We will elaborate on these points below. First, we describe in § 2 the *IUE* spectrum of PG 1148+549. In § 3 we present our measurements of the lines and discuss possible alternatives to the Ne VIII λ774 identification. In § 4 we describe theoretical equilibrium models of the emission-line gas. We also discuss the criteria for cloud stability and make specific predictions for the Ne VIII and other doublet emission line ratios. In § 5 we reaffirm the Ne VIII identification in the context of the line-strength predictions. In § 6 we estimate the covering factor and physical conditions in the Ne VIII emission regions, and we note the possible relationship to other highly ionized emission/absorption regions in AGNs. In § 7 we summarize the main results.

2. THE *IUE* ARCHIVE SPECTRA

Figure 1 shows the co-added, optimally extracted spectrum of PG 1148+549 obtained from the *IUE* atlases of Kinney et al. (1991) and Lanzetta et al. (1993). The plot combines the separate short- and long-wavelength *IUE* spectra, which join without overlap at ~1970 Å. We rebinned the spectra on a linear wavelength scale (~1.2 Å pixel^{-1}) for processing with IRAF and then applied a 3 pixel–wide boxcar smoothing function to display better the BELs. We also removed several narrow spectral artifacts identified by Kinney et al. (1991). The plotted spectrum represents total exposure times of 16.5 hr for $\lambda < 1970$ Å and 13.3 hr for $\lambda > 1970$ Å. The slight continuum discontinuity in Figure 1 near 1970 Å is probably due to a mismatch between the long- and short-wavelength flux calibrations. The FWHM resolution is roughly 6 Å. The final spectrum looks very much like that shown (and reduced independently) by Koratkar, Kinney, & Bohlin (1992).

3. LINE MEASUREMENTS AND IDENTIFICATIONS

Figure 1 also shows a low-order polynomial fit to the continuum and single Gaussian fits to each line. The Gaussian fits provide estimates of the line strengths and widths and separate estimates for the blended Lyα and N V lines. The results from the fitting are given in Table 1, where λ_{obs} is the observed line-centroid wavelength, λ_{rest} is the corresponding rest wavelength with the assumption that $z_e = 0.978$ (from C III] and Mg II; Tytler & Fan 1992), z_{em} is the redshift derived by us from each Gaussian line centroid, Δv is the velocity shift of these centroids from $z_e = 0.978$, W_λ^{rest} is the rest equivalent width, F is the flux, and FWHM is the full width at half-maximum of the Gaussian fits. The uncertainties in these quantities are dominated by systematic effects, including nonstatistical fluctuations in the reduced spectra and the subjective, schematic fits to both the lines and continuum. The quality of the measurements can best be judged by inspection of Figure 1. We expect that the actual 1 σ uncertainties in the line strengths and widths are about 10%–20%, although the blended Lyα and N V lines are more uncertain. The centroid

TABLE 1

LINE FITTING RESULTS

Line	λ_{obs} (Å)	λ_{rest} (Å)	z_{em}	Δv (km s^{-1})	W_λ^{rest} (Å)	F (10^{-14} erg cm^{-2} s^{-1})	FWHM (km s^{-1})
Ne VIII λ774.....	1502.0	759.4	0.941	5600	6.2	13.5	7000
O VI λ1034	2026.7	1024.6	0.959	2800	5.9	10.0	3800
Lyα[a].....	2393.4	1210.0	0.969	1400	45.2	62.0	9500
N V λ1240[a].....	2440.4	1233.8	0.968	1500	22.0	30.2	8200
Si IV + O IV].....	2761.4	1396.1	...	...	6.6	7.5	3900
C IV λ1549	3033.0	1433.7	0.958	3000	21.0	22.0	7000

[a] Measurements listed for Lyα and N V are very uncertain because the lines are severely blended.

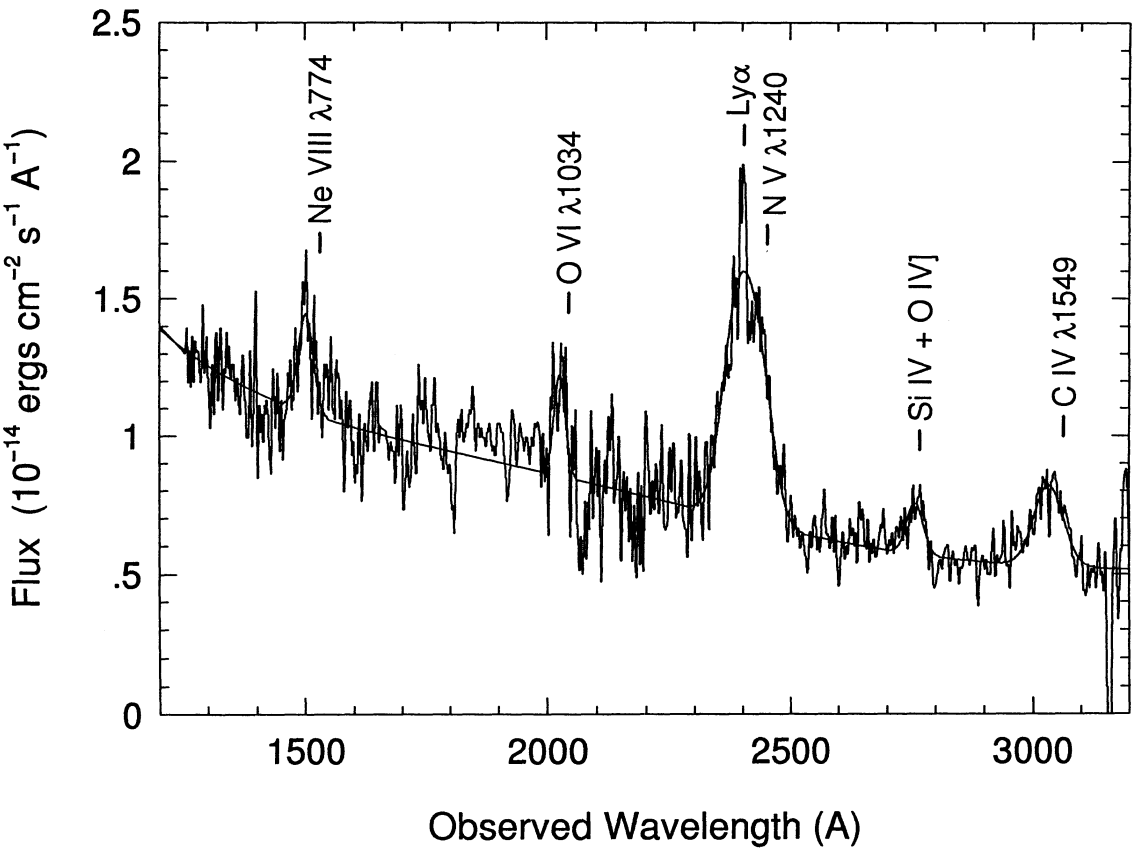

FIG. 1.—Co-added *IUE* spectra of PG 1148+549 plotted at the observed wavelengths. The short- and long-wavelength data join without overlap at ~1970 Å, which causes a slight discontinuity in the plotted continuum. The spectra are smoothed with a 3 pixel–wide boxcar function. The prominent emission lines are labeled at the published redshift of $z_e = 0.978$. The smooth, solid line is a polynomial fit to the continuum, with single Gaussian fits to each of the labeled lines. The Ne VIII and C IV velocity widths are similar despite their different appearances in this figure.

wavelengths of the unblended lines probably have 1 σ uncertainties of $\sim\frac{1}{3}$ the half-width of the Gaussians.

Note that all of the line centroids are substantially blueshifted from z_e as measured by Tytler & Fan (1992). Also note that the doublet splitting in Ne VIII and O VI (3850 and 1650 km s^{-1}, respectively) could affect their measured line widths and positions. We did not attempt to separate the flux in these doublets or in the possible blends of O VI λ1034 with Lyβ or S IV λ1397 with O IV] λ1402.

Secure measurement of the ~1500 Å emission line in PG 1148+549 will require data with higher resolution and signal-to-noise ratio. In particular, *IUE* spectra can have spurious broad emission—of unknown origin, but presumably intrinsic to the *IUE* satellite—near 1500 Å (Crenshaw, Bruegman, & Norman 1990). *IUE* spectra of QSOs (Kinney et al. 1991; Koratkar et al. 1992) sometimes show a broad feature at ~1500 Å that cannot be identified with a line in the QSO. However, those spurious features do not look like QSO emission lines; they are broader, less symmetric, and broken into multiple peaks (see Crenshaw et al. 1990 and Koratkar et al. 1992). In PG 1148+549, the ~1500 Å feature is stronger (relative to the continuum) and more "linelike" in appearance than the artifacts in other sources. We therefore expect that this measured line is intrinsic to the QSO.

PG 1148+549 thus joins the list of several QSOs known to have a probable Ne VIII λ774 emission line (Hamann et al. 1995b). In the highest quality existing spectrum, that of PG 1522+101 (Cohen et al. 1995), the feature is very strong but too broad to clearly implicate Ne VIII. Line-profile fitting by Cohen et al. (1995) shows that Ne VIII λ774, with the assumption that it has the same redshift and profile as C IV λ1549, provides the best single-line match to the feature in PG 1522+101. However, the fits are not good, and large contributions from other lines cannot be not ruled out. Unfortunately, these attempts at identification based solely on the line profiles and redshifts are compromised by the possibilities for instrinsic differences between different lines. In particular, Ne VIII might form in a different region that the lower ionization lines (see § 6.1) and thus have a very different profile or redshift.

Alternatives to the Ne VIII λ774 identification include N IV λ765, O IV λ789, S V λ786, and Ar VI λ763. The theoretical strengths of these lines are discussed in §§ 4 and 5; we will argue from those calculations that Ne VIII λ774 is the most likely contributor to emission near this wavelength, but here we simply note that attributing the ~1500 Å feature in PG 1148+549 to Ne VIII λ774 implies a velocity shift (Table 1) that follows the usual progression for smaller redshifts in higher ionization lines, although the magnitude of the shift may be unusually large (Gaskell 1982; Espey et al. 1989; Tytler & Fan 1992).

4. MODELS OF THE LINE-EMITTING REGIONS

Here we examine the conditions in the line-emitting regions using the spectral synthesis code CLOUDY, version 87.23

(Ferland 1995). We consider both photoionization and collisional (coronal) equilibrium scenarios. The local Doppler line widths, which affect the line optical depths and continuum scattering, are assumed to be thermal. The line radiative transfer is handled through escape probabilities, which include the continuum opacities. Dust grains are excluded because they are not expected to survive in the regions of interest. The elemental abundances are solar (Grevesse & Anders 1989), except as noted. Solar abundances for a $z_e \sim 1$ QSO are consistent with the emission-line analysis of Hamann & Ferland (1992, 1993) and Baldwin et al. (1995). The Ne/O ratio, which affects the relative Ne VIII λ774 and O VI λ1034 line strengths, should be close to solar in any case because these elements form together in massive-star supernovae (Timmes, Woosley, & Weaver 1995). Experiments show that the abundances could be changed by factors of at least several without affecting any of the important conclusions in this paper.

4.1. *Photoionized Gas*

The photoionization calculations assume constant-density, plane-parallel clouds illuminated on one face. The incident continuum is from Mathews & Ferland (1987), with an additional break at 1 μm to lessen the flux at longer wavelengths. The change in continuum slope from $\alpha = 1$ to $\alpha = 2.5$ at longer wavelengths (where $f_\nu \propto \nu^\alpha$) minimizes the free-free heating (Ferland & Persson 1989; Ferland et al. 1992) and is consistent with recent theories that attribute the observed near-IR continua to dust emission outside the BELR radius (Sanders et al. 1989). The Mathews & Ferland (1987) spectrum includes a typical BBB, whose strength relative to the X-rays corresponds to $\alpha_{ox} = -1.4$ (where α_{ox} is the spectral index that would connect the continuum flux between 2500 Å and 2 keV). The only published X-ray observations of PG 1148+549 known to us (Della Ceca et al. 1990) provide a 3 σ upper limit corresponding to $\alpha_{ox} < -1.1$ when compared to the *IUE* flux extrapolated to $\sim$2500 Å rest (Fig. 1).

The total hydrogen space and column densities are fixed throughout the calculations at $n_H = 10^{11}$ cm^{-3} and $N_H = 10^{24}$ cm^{-2}, respectively. (In practice, low-ionization models are truncated at the column where the gas recombines, i.e., where the electron fraction drops below 0.75, and the gas becomes too cool to emit in Lyα and the high-ionization lines discussed here.) The choice of n_H is motivated by recent estimates for the BELR in the variable Seyfert 1 galaxy NGC 5548 (Ferland et al. 1992). Our results are not sensitive to the choice of n_H, except for lines such as C IV that are very optically thick and collisionally de-excited. These thermalization effects are discussed in § 4.4.

Some predicted line strengths are shown in Figure 2 for a range of ionization parameters U—defined as the dimensionless ratio of the ionizing photon ($\lambda < 912$ Å) to total hydrogen (H I + H II) densities at the illuminated face of the clouds. The line strengths are expressed as equivalent widths, W_λ, relative to the incident continuum for emitting regions that completely cover the central source.[2] Equivalent widths for lesser covering derive from Figure 2 by multiplication by the covering factor,

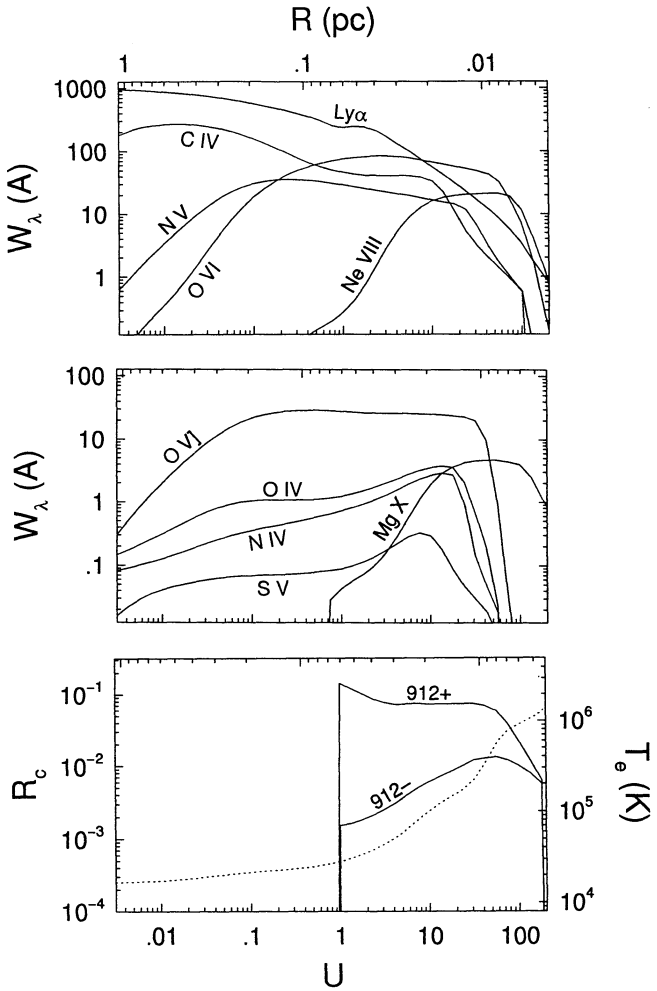

FIG. 2.—Photoionization results plotted for various ionization parameters (U). The calculations use a standard AGN continuum and space and column densities of $n_H = 10^{11}$ cm^{-3} and $N_H = 10^{24}$ cm^{-2}, respectively. The radii across the top are the distances from the continuum source required to be consistent with the measured flux at 912 Å rest (Fig. 1) and the redshift $z_e = 0.978$ in a cosmology with $H_0 = 75$ km s^{-1} Mpc^{-1} and $q_0 = 0.25$. The top two panels show predicted line equivalent widths (W_λ, in Å) measured relative to the incident continuum. The lines are Lyα, C IV λ1549, N V λ1240, O VI λ1034, Ne VIII λ774, N IV λ765, O IV λ789, O V] λ1218, S V λ786, and Mg X λ615. The bottom panel shows the electron temperature (T_e) at the illuminated face of the clouds (*dotted line—right scale*) and the ratio (R_c) of the diffuse to incident continuum fluxes on either side of the Lyman edge (912+ and 912− Å) for that part of the total column responsible for Ne VIII emission (*solid lines—left scale*).

$q \equiv \omega/4\pi$, where ω is the solid angle subtended by the clouds as seen from the continuum source. We emphasize that the equivalent widths for a fixed U do *not* depend on the density unless line thermalization is important. The bottom panel of Figure 2 shows the electron temperature, T_e, at the illuminated face of the clouds. In all cases, the temperature and ionization decline with increasing depth into the clouds. For $U \gtrsim 2$, the clouds are fully ionized (H II), and for $U \gtrsim 10$, the entire column is optically thin to bound-free absorption at the H I Lyman edge (912 Å). The electron scattering optical depth reaches a maximum of $\sim$0.7 when the clouds are fully ionized ($U \gtrsim 2$).

The bottom of Figure 2 also shows the thermal, diffuse (bound-free + free-free), continuous emission from *just* the column of gas needed to form Ne VIII λ774. Specifically, this is

[2] In our calculations, the *geometric* covering factor is unity but the *radiative* covering is zero. That is, by assumption, Ne VIII λ774 photons escaping locally are not absorbed by clouds at different locations, even if the Lyman continuum in those clouds is optically thick. This simplification only strengthens the lower limit to the Ne VIII covering factor derived in § 6.1.

the column, measured from the front face of the clouds, that includes 95% of the total Ne VIII flux. This column equals 10^{22} cm^{-2} at $U \approx 1.6$, 10^{23} cm^{-2} at $U \approx 12$, and 10^{24} cm^{-2} at $U \gtrsim 65$. The diffuse continuum flux at 912 Å is plotted as a ratio, R_c, relative to the incident continuum. This ratio, like the line equivalent widths, applies for complete covering ($q = 1$). Since there is no Lyman discontinuity in the incident spectrum, the different values of R_c on either side of 912 Å are due solely to the local, diffuse bound-free edge.

Figure 3 plots the line equivalent widths (*upper panels*) for a range of total column densities and a fixed ionization parameter $U = 10$. This figure shows that Ne VIII is fully formed (i.e., the zone of Ne VIII emission is fully within the clouds) for columns $N_H \gtrsim 10^{23}$ cm^{-2}. Thus, in our simulations with $U = 10$ and $N_H = 10^{24}$ cm^{-2}, Ne VIII λ774 forms entirely within the first $\sim 1/10$ of the total column, measured from the illuminated face. Lower ionization lines form mostly or entirely at larger columns. The bottom panel of Figure 3 shows T_e and the diffuse continuum emission coefficient, γ_ν (Osterbrock 1989, p. 88), as functions of the column into a single cloud with $U = 10$ and total column density $N_H = 10^{24}$ cm^{-2}. Note that

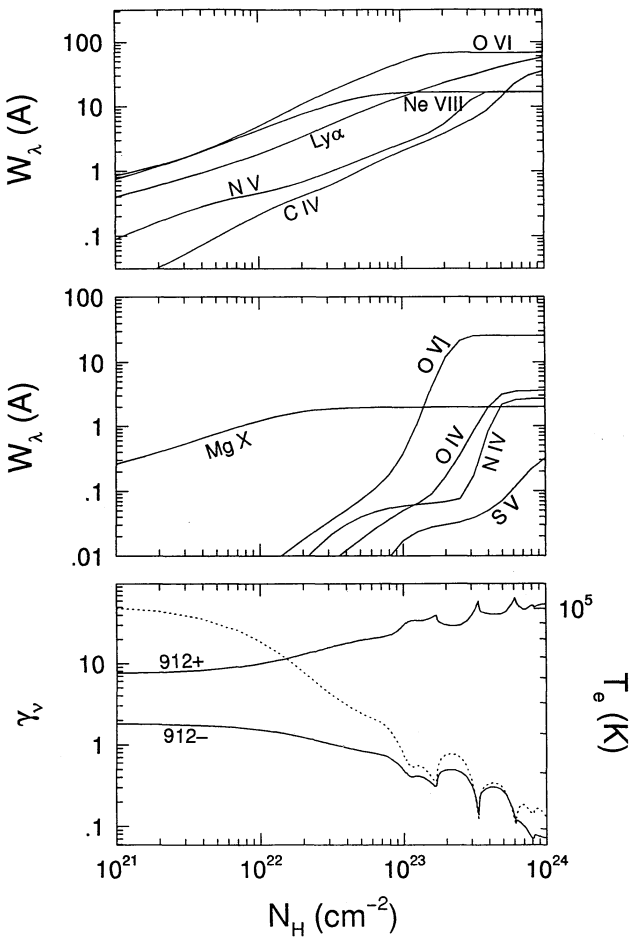

FIG. 3.—Photoionization results for $U = 10$ plotted for clouds of different column densities (*top*, *middle*) and as a function of the column density into a single cloud (*bottom*). All other parameters are the same as the $U = 10$ calculation in Fig. 2. The top two panels show the line equivalent widths. The bottom panel shows the electron temperature (*dotted line—right scale*) and the continuous emission coefficient (γ_ν, in units of 10^{-40} ergs cm^3 s^{-1} Hz^{-1}) on either side of the Lyman edge (912+ and 912− Å; *left scale*).

γ_ν shows a greater Lyman discontinuity at the lower temperatures attained at large columns. Indeed, most of the diffuse continuum short of the Lyman edge derives from the cool regions at large columns and *not* from the Ne VIII–emitting gas. (This point will become relevant in § 6.3.)

4.2. *Collisionally Ionized Gas*

Although there is strong evidence for photoionization throughout the BELR (e.g., correlated line and continuum variabilities; see Peterson 1993 for a review), we cannot rule out significant mechanical heating in the newly recognized Ne VIII region. We therefore show in Figure 4 the predicted line and continuum emissions from a slab of gas that is collisionally ionized at various equilibrium temperatures. The incident continuum is assumed to be negligible in this case, so both the ionization and line excitation are controlled by collisions and

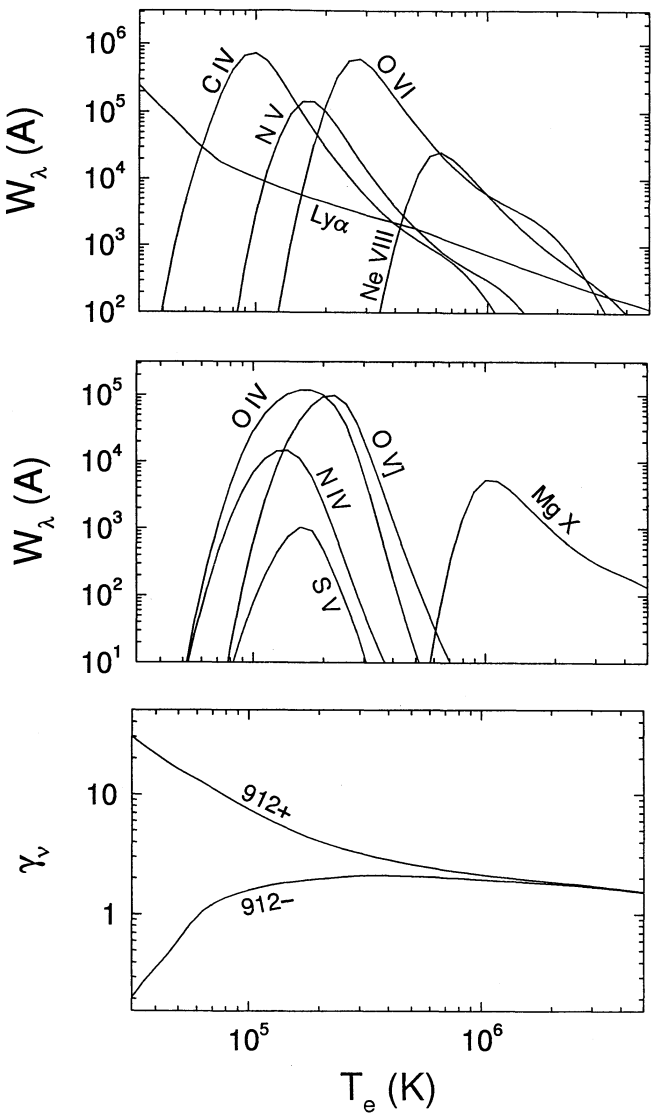

FIG. 4.—Collisional equilibrium results plotted as a function of the equilibrium temperature (T_e) for the case in which $n_H = 10^9$ cm^{-3} and the lines and continua are optically thin throughout. The top two panels show several line equivalent widths measured relative to the diffuse continuum emitted by the same gas. The bottom panel shows the continuous emission coefficient (γ_ν, in units of 10^{-40} ergs cm^3 s^{-1} Hz^{-1}) on either side of the Lyman edge. See Fig. 2.

charge-exchange reactions. Unlike the photoionized models above, the lines and diffuse continua are assumed to be optically thin in Figure 4. This situation is like that described by Stern, Wang, & Bowyer (1978), Shull & Van Steenberg (1982), Gaetz & Salpeter (1983), Arnaud & Rothenflug (1985), and others. The line strengths are plotted as equivalent widths relative to the diffuse continuum emitted by the same gas. The results apply for any density relevant to this discussion, as long as the combined space and column densities are not large enough to thermalize the lines. Note that the line equivalent widths are much larger in Figure 4 than in Figure 2 because the diffuse continuum is weak compared to the incident flux in the photoionized cases. Also, several lines, such as C IV and O VI, are much stronger relative to Ne VIII (at their peaks) in Figure 4 because of the lack of thermalization.

4.3. *Stability of the* Ne VIII *Gas*

The high temperatures and ionizations in the Ne VIII region can make that gas unstable to changes in temperature or density. It is well known that collisionally ionized gas is generally thermally unstable for temperatures 3×10^5 K $\lesssim T_e \lesssim 3 \times 10^7$ K (e.g., Field 1965; Gehrels & Williams 1993). These instabilities occur because the line cooling becomes less efficient as the temperature and ionization increase over this range. However, there are narrow windows of stability for T_e centered at $\sim 8 \times 10^5$ K and $\sim 5 \times 10^6$ K (Gehrels & Williams 1993). Figure 4 shows that the Ne VIII emission (and ionization fraction) peaks near the local stability at $\sim 8 \times 10^5$ K. Therefore, considerable Ne VIII emission *could* form in stable, collisionally ionized gas.

In photoionized gas, the temperature decouples from the ionization, and a different analysis must be used. We examine the stability of photoionized gas by considering changes in the gas pressure that occur when the density is perturbed. This analysis and the results below are consistent with the more detailed studies by Krolik, McKee, & Tarter (1981), Kallman & Mushotzky (1985), Netzer (1990), and Marshall et al. (1993). Our calculations are performed at a fixed incident flux using the same ionizing spectrum as in § 4.1. For simplicity, we assume the lines and continuum are optically thin. (Substantial column densities would only complicate the presentation because such clouds would contain a range of temperatures and ionizations and, if the pressure is forced to be constant throughout each cloud, the clouds would also have a range of densities.) Figure 5 shows the pressure $n_e T_e$ versus density n_H (*bottom scale*) and U (*top scale*) for different metallicities. The abundances have solar ratios (Grevesse & Anders 1989), except in the $Z = 5\ Z_\odot$ case, where nitrogen is 15 times solar (i.e., N/O = 3 times solar) to mimic the large secondary N production expected at high Z's (Hamann & Ferland 1993). The incident flux was chosen so that $U = 10$ at $n_H = 10^{11}$ cm^{-2}. However, the fundamental quantity is actually U because it sets the ionization. Repeated experiments show that the same pressure-versus-U behavior applies for a wide range of fixed fluxes and corresponding density scales. Note that T_e is sometimes higher at high metallicities and large U (Fig. 5) because the metals increase the X-ray continuum opacity (heating) without a commensurate increase in the line emission (cooling).

Photoionized gas is unstable if the pressure decreases with increasing n_H, i.e., if $d(n_e T_e)/d(n_H)$ is negative in Figure 5. Comparing Figures 2 and 5 shows that the range of U's needed for Ne VIII overlaps with the pressure instability at $30 \lesssim U \lesssim 60$. This instability corresponds to an abrupt change in temperature from $\sim 2 \times 10^5$ K to nearly 10^6 K for $Z \gtrsim 1\ Z_\odot$. Figure 2 suggests that Ne VIII emission may come from large-column-density clouds with $U > 60$; however, the unstable transition from $T_e \sim 10^6$ K to $T_e \sim 10^5$ K will occur somewhere in those clouds, making them unstable. Thus, *if* the emission lines come from stable clouds, Ne VIII λ774 will form only over the narrow range $5 \lesssim U \lesssim 30$—where the ionization is high enough for Ne VIII and the clouds are stable throughout.

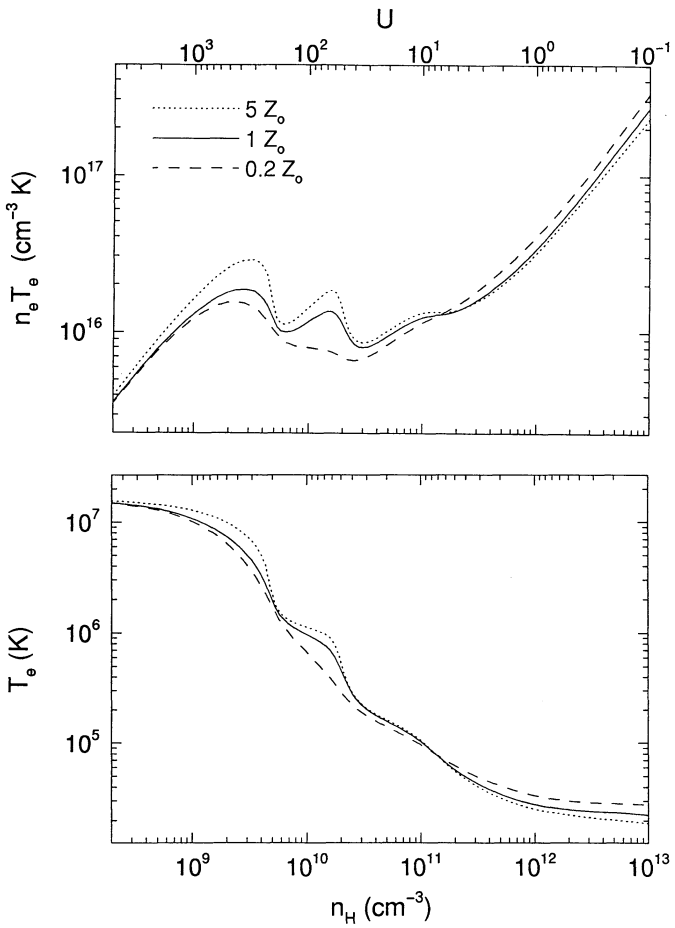

FIG. 5.—Gas temperature (T_e) and pressure ($n_e T_e$) plotted against the density (n_H) and ionization parameter (U) for optically thin, photoionized gas with metallicities of 0.2 (*dashed line*), 1 (*solid line*), and 5 (*dotted line*) $Z_\odot$. The shapes of the curves depend only on U. The density scale across the bottom depends on the incident ionizing flux, assumed here to be 3×10^{22} photons cm^{-2} s^{-1} for $\lambda < 912$ Å.

4.4. *Line Optical Depths and Thermalization*

Reasonable space and column densities in the BELR can lead to line fluxes that are significantly reduced by photon trapping and collisional de-excitation (Davidson & Netzer 1979; Ferland et al. 1992). These thermalization effects can impact both the line ratios and overall strengths. The criterion for significant collisional de-excitation is $n_e C_{ul} \gtrsim \beta A_{ul}$, where n_e is the electron density, C_{ul} is the downward collisional rate coefficient, β is the line escape probability, and A_{ul} is the spontaneous radiative decay rate. For large line-center optical depths, $\tau_0 \gg 1$, the escape probability is roughly $\beta \sim 1/\tau_0$ (Frisch 1984), and the condition for collisional de-excitation can be written as $n_e \tau_0 \gtrsim A_{ul}/C_{ul}$. The ratios A_{ul}/C_{ul} at tem-

TABLE 2

LINE THERMALIZATION THRESHOLDS

TRANSITION	$A_{ul}/C_{ul} \approx n_e \tau_0$ 20,000 K (cm^{-3})	$A_{ul}/C_{ul} \approx n_e \tau_0$ 200,000 K (cm^{-3})
Mg X λ615	3.2E16	9.7E16
Ne VIII λ774.....	1.6E16	5.0E16
O VI λ1034.....	7.6E15	2.2E16
N V λ1240.....	4.7E15	1.4E16
C IV λ1549	3.0E15	7.5E15
N IV λ765	3.2E16	1.0E17
O IV λ789	2.3E16	7.3E16

peratures $T_e = 2 \times 10^4$ K and 2×10^5 K are listed in Table 2 for several lines using atomic data from Wiese, Smith, & Glennon (1966), Mendoza (1983), and Cochrane & McWhirter (1983).

Figure 6 shows the total line-center optical depths for the photoionized clouds in Figures 2 and 3, where $n_e \approx n_H = 10^{11}$ cm^{-3}. Comparisons with the critical values of $n_e \tau_0 \approx A_{ul}/C_{ul}$ in Table 2 confirm that thermalization effects can be important. For example, in our photoionized simulations (§ 4.1), C IV can be collisionally suppressed by factors greater than 100, but Ne VIII is suppressed by $\gtrsim 30\%$.

Measurements of line ratios within resolved multiplets can place constraints on the amount of thermalization and, thus, the product $n_e \tau_0$. The resonant "lines" Mg X λ615, Ne VIII λ774, O VI λ1034, N V λ1240, and C IV λ1549 are actually doublets with identical lithium-like term structures. We calculate these doublet emission ratios by solving the detailed balance equations for three-level atoms, using escape probabilities $\beta \sim 2/\tau_0$ for the midplane of an emitting slab in the limit $\tau_0 \gg 1$. The collision strengths connecting the two upper states, $2p^2P^0_{3/2} \rightarrow 2p^2P^0_{1/2}$, are not known, but we assume their strengths are equal to $\frac{1}{4}$ of the $2p^2P^0_{3/2} \rightarrow 2s^2S_{1/2}$ resonant collision strengths (see Mendoza 1983). The resulting doublet ratios are shown in Figure 7 as functions of the product $n_e \tau_0$, where τ_0 is the summed doublet optical depth. The predicted ratios are the same if either n_e, τ_0, or both parameters are considered to change. The results are, though, sensitive to the assumed $2p^2P^0_{3/2} \rightarrow 2p^2P^0_{1/2}$ collision strength. If Ω is the actual collision strength and Ω_0 is the value used in Figure 7, then situations where $\Omega > \Omega_0$ would shift the curves to the left by factors $\sim(\Omega/\Omega_0)^{1/2}$, but $\Omega < \Omega_0$ would shift the curves to the right by no more than a factor of ~ 1.6 (which is the limit corresponding to $\Omega = 0$).

Figure 7 shows that the lithium-sequence ratios vary from $\sim 2:1$ at low $n_e \tau_0$ to $\sim 1:1$, where the levels thermalize, at large $n_e \tau_0$. The Ne VIII and Mg X doublets deviate from this simple behavior at low temeratures because the larger energy splitting

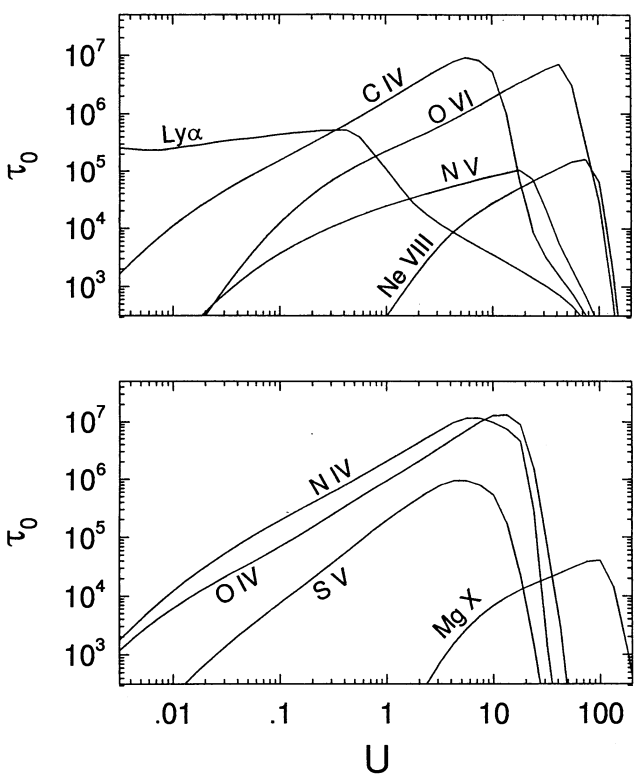

FIG. 6.—Total line-center optical depths (τ_0) measured across the full radial extent of the modeled clouds plotted for various ionization parameters (U) in the photoionized scenarios from Fig. 2.

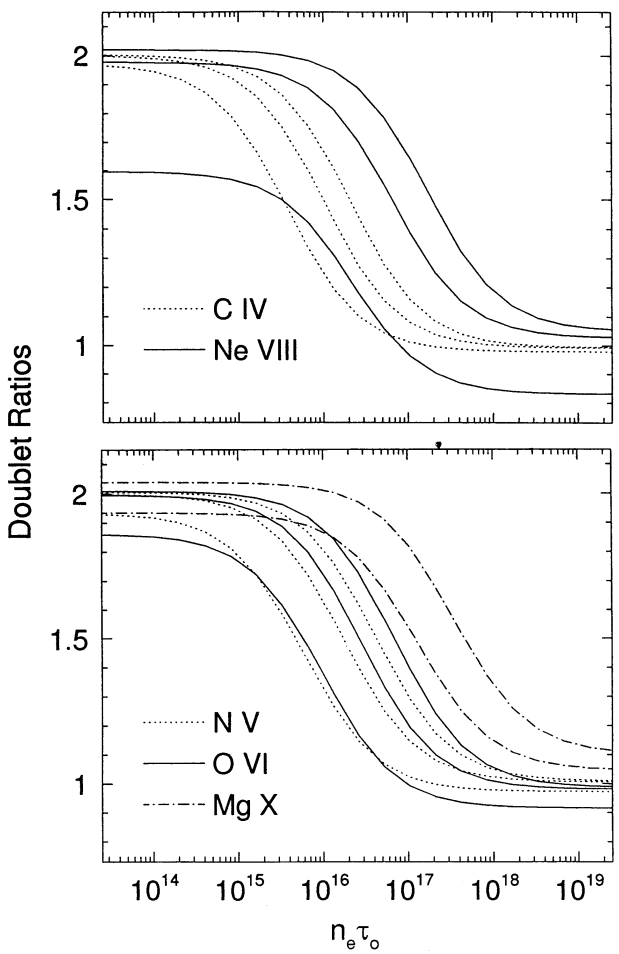

FIG. 7.—Doublet emission ratios for Ne VIII λ770/λ780 and C IV λ1548/λ1550 (*top*) and for N V λ1238/λ1242, O VI λ1031/λ1037, and Mg X λ610/λ625 (*bottom*) plotted against the product of the line optical depth and electron density ($n_e \tau_0$, in cm^{-3}). The results are identical if either n_e or τ_0 is considered to vary. The three curves for each ratio correspond to $T_e = 10^4$, 10^5, and 10^6 K from bottom to top (or right to left), except for Mg X, where $T_e = 10^4$ K is not shown.

of their upper states makes them more temperature sensitive. Nonetheless, in our photoionization calculations (§ 4.1), Ne VIII λ770/λ780 and Mg X λ610/λ625 are $\sim$2:1 for all values of U, while C IV λ1548/λ1550 is nearly 1:1 for $U \gtrsim 0.2$ (compare Figs. 2, 6, and 7). Resolved measurements of the more widely separated doublets would test these predictions and constrain the space and column densities (the product $n_e \tau_0$) in the emitting gas.

5. Ne VIII λ774 VERSUS ALTERNATIVE IDENTIFICATIONS

The strongest known alternatives to the Ne VIII λ774 identification are included in our calculations and shown in Figures 2–4. (Collision strengths for Ar VI λ763 are not available, but given the assumption that those strengths are comparable to Ne VIII, simple abundance considerations predict maximum Ar VI fluxes less than 1/10 of Ne VIII at its peak.) The strongest of the alternative lines are O IV λ789 and N IV λ765. Their strengths relative to Ne VIII can depend on the geometry because they form in distinct regions of lower ionization (Figs. 3 and 4; see also Hamann et al. 1995a). For example, highly ionized clouds could emit exclusively in Ne VIII, but photoionized clouds could also produce N IV and O IV at large column densities while emitting Ne VIII near the illuminated face. In our calculations with $N_H = 10^{24}$ cm^{-2} and $U \lesssim 20$, all three of these lines are fully formed (i.e., their ionization zones are fully within the clouds), so increasing the column would not affect the derived line strengths, but lowering the column would make N IV and O IV weaker relative to Ne VIII (Fig. 3). Therefore, for any $U \gtrsim 2$ the flux in Ne VIII exceeds that in N IV and O IV, and Ne VIII λ774 is the most likely identification in this highly ionized regime.

At lower U in the photoionized simulations (Fig. 2), N IV and O IV are never stronger than a few percent of C IV, and their equivalent widths are $\lesssim$1 Å even if the covering factor is unity. Thus, N IV and O IV appear to be too weak to account for the features measured near 774 Å (rest) in PG 1148+549 and other QSOs (Hamann et al. 1995b; Cohen et al. 1995). This result is not sensitive to the geometry and total column density because the three lines C IV, N IV, and O IV form in overlapping zones (Figs. 2–4; Hamann et al. 1995a). At lower space densities, C IV would be less thermalized, which would make N IV and O IV relatively weaker and even less viable as identifications. At very high densities, the line ratios are forced toward unity due to severe thermalization (§ 4.4), but densities greater than 5×10^{12} cm^{-3} would be needed in the photoionized models to make N IV and O IV nearly as strong as C IV.

Therefore, N IV λ765 and O IV λ789 should be too weak compared to both C IV λ1549 and the continuum at low U, and compared to Ne VIII at high U. We conclude that, even without the line profile or centroid considerations (§ 3; Cohen et al. 1995), Ne VIII λ774 is the most likely identification for strong emission near this wavelength.

6. DISCUSSION: THE Ne VIII λ774–EMITTING REGION

6.1. *Geometry and Physical Conditions*

The presence of Ne VIII λ774 emission requires a BELR component that is more highly ionized and probably much hotter than previously recognized. If the gas is photoionized by a standard AGN continuum, the Ne VIII equivalent width, the Ne VIII/O VI line ratio (Table 1 and Fig. 2), and the assumption of pressure stability (Fig. 5) imply ionization parameters of $5 \lesssim U \lesssim 30$. (Although the predicted Ne VIII/O VI ratio in Fig. 2 is somewhat lower than the measured value, this difference is readily accounted for by the measurement uncertainties and the schematic nature of the calculations.) The temperatures in the Ne VIII zone are predicted to be in the range 5×10^4 K $\lesssim T_e \lesssim 2 \times 10^5$ K. In collisional equilibrium (Fig. 4), the temperatures would lie near $\sim 8 \times 10^5$ K in thermally stable clouds.

Models of the BELR based on N V, C IV, Lyα, and lower ionization lines have typically led to estimates of $U \lesssim 0.1$ and $T_e \lesssim 2 \times 10^4$ K for photoionization by continua similar to that used here (Davidson & Netzer 1979; Kwan & Krolik 1981; Ferland & Persson 1989; Ferland et al. 1992; Shields & Ferland 1993; Baldwin et al. 1995; Rosenblatt et al. 1995). Calculations that consider also the higher ionization O VI λ1034 line can require BELR components with $U \gtrsim 1$ (Hamann & Ferland 1992). The Ne VIII λ774 emitting zone might be just an extension of this more familiar BELR, with the higher temperatures and ionizations caused by lower densities and/or closer proximity to the continuum source. The difference between $U \gtrsim 5$ in the Ne VIII zone and $U \lesssim 0.1$ in the standard C IV–Lyα region could be caused by a factor of $\gtrsim$7 difference in distance for a fixed density or a $\gtrsim$50 difference in density at a given distance (Fig. 2). Obviously, some mixture of lower densities and distances could also apply to the Ne VIII gas. The tentative measurement of a lower redshift in Ne VIII compared to C IV and probably O VI in PG 1148+549 (§ 3) supports the suggestion of the spatial segregation of these regions.

The photoionization results indicate that the large Ne VIII equivalent width in PG 1148+549 requires covering factors $q \gtrsim \frac{1}{3}$ (Fig. 2) and total column densities $N_H \gtrsim 10^{22}$ cm^{-2} (Fig. 3). The minimum q applies if the column density is large enough to fully encompass the Ne VIII–emitting zone, while the minimum N_H applies if $q = 1$. Larger q and N_H would be needed if some of the line flux were absorbed by dust or neutral gas (H I—see footnote 2). The limits on q and N_H are not sensitive to the space density because Ne VIII is not thermalized in our calculations for densities $n_e \lesssim 10^{11}$ cm^{-3}. At much higher densities, where Ne VIII does thermalize, the limits on both q and N_H would increase by, for example, a factor of $\sim$2 for $n_H = 5 \times 10^{12}$ cm^{-3}.

6.2. *X-Ray and UV Absorption Properties*

The Ne VIII λ774 emitting gas will appear as an X-ray warm absorber if it lies along our line of sight to the X-ray continuum source (Netzer 1993; Shields et al. 1995; Hamann et al. 1995a). Warm absorbers can be identified by O VII or O VIII bound-free absorption edges at roughly 0.8 keV. In the Ne VIII–emitting region, O VII and O VIII are the dominant species of oxygen (e.g., Hamann et al. 1995b), and the column density derived above for the Ne VIII–emitting gas, $N_H \gtrsim 10^{22}$ cm^{-2}, will produce optical depths of at least a few at the O VII–O VIII edge (Morrison & McCammon 1983; Arnaud & Rothenflug 1985). Furthermore, photoionized gas with these total columns and $U \gtrsim 5$ will exhibit another defining property of the warm absorbers, namely, the X-ray bound-free opacity is sensitive to changes in the incident (ionizing) flux (Shields et al. 1995). The large covering factor estimated for the Ne VIII gas in PG 1148+549 ($q \gtrsim \frac{1}{3}$) suggests that there is a realistic chance to measure X-ray absorption caused by viewing the Ne VIII BELR along our line of sight to the continuum source.

The connection between Ne VIII emission and the X-ray warm absorbers is bolstered by recent measurements of soft

X-ray O VII–O VIII or ~88 Å Ne VII–Ne VIII emission lines in two low-luminosity AGNs known to have O VII–O VIII absorption edges (George et al. 1995; Kaastra et al. 1995). The calculations by George et al. (1995), in particular, show that the O VII–O VIII emission and absorption features could both naturally form in the same gas. We note that this gas should also produce Ne VIII λ774 emission.

This highly ionized, emitting gas could further produce associated ($z_a \approx z_e$) absorption lines if it lies along our line of sight to the continuum source. This expectation is tempered only by our prediction that the Ne VIII emission line is optically thick (Fig. 5); so, in absorption, it should be on the flat part of the curve of growth, with an equivalent width depending on the local Doppler velocities. Nonetheless, Hamann et al. (1995a) showed that for reasonable Doppler parameters, $b \gtrsim 20$ km s^{-1}, substantial Ne VIII absorption equivalent widths, $W_\lambda \gtrsim 0.3$ Å, will occur if Ne VIII is near its maximum ionization fraction and the total column is $N_{\rm H} \gtrsim 10^{21}$ cm^{-2} (for solar abundances). The measurement of associated Ne VIII λ774 absorption within 200 pc of one QSO, UM 675 (Hamann et al. 1995a), shows directly that $z_a \approx z_e$ absorbers can have physical conditions appropriate for both X-ray warm absorption and Ne VIII emission (although, in UM 675, the Ne VIII column along our line of sight is too low for significant line emission).

A simple model would place all of the highly ionized absorbing gas in the same general region—in or near the Ne VIII BELR. One obstacle to this unified picture might be that the associated absorption lines sometimes appear to form outside the BELR because they absorb both the continuum and the emission lines (especially Lyα; Hamann et al. 1995a; Mathur 1994; Mathur et al. 1994). This apparent conflict is overcome if the emission lines (e.g., Lyα) are preferentially beamed back toward the continuum source (Ferland et al. 1992). In this case, the emission and absorption regions could be intermixed because most of the emission comes from the far side of the BELR, on the other side of the AGN (Shields 1994).

6.3. *Diffuse Continuum Emission and the Big Blue Bump*

The calculations in § 4 indicate that Ne VIII emission/absorption regions have temperatures somewhere in the range 5×10^4 K $\lesssim T_e \lesssim 10^6$ K (see also Hamann et al. 1995a), which is roughly the range needed for the thermal-reprocessing models of the BBB (Malkan & Sargent 1982; Barvainis 1993). Here we examine whether the optically thin, Ne VIII–emitting gas could be the source of the BBB.

Kriss (1995) showed that in a hot plasma that is optically thin in both the lines and continuum, the prominent UV lines have equivalent widths relative to the diffuse continuum of greater than 1000 Å. Those estimates are supported by our collisional-equilibrium results in Figure 4. Clearly, if this gas produced the BBB in AGNs, the lines sitting atop the BBB would be many times stronger than observed. To reconcile this problem, some mechanism(s) must be invoked to weaken the lines relative to the diffuse continuum. Large electron scattering optical depths could broaden the lines and make them harder to detect. However, this scattering would not destroy line photons, and Kriss (1995) has argued that the broadening is not sufficient to limit their strong detection. Another possibility is line thermalization. Large line opacities could weaken the lines while the continuum remained optically thin. However, our calculations for $n_{\rm H} = 10^{11}$ cm^{-3} show that even if the column densities were at their maximum allowed by an optically thin continuum (at the Lyman edge), the line optical depths would be no more than a few times larger than their maximum values shown in Figure 6, and the prominent lines (including Ne VIII) would still have equivalent widths greater than 1000 Å. We find that, in collisional equilibrium, densities $\gtrsim 5 \times 10^{13}$ cm^{-3} would be needed to adequately weaken the lines relative to the continuum via thermalization. (Note that the densities for adequate thermalization would be even higher if the line optical depths were lowered by turbulence within the clouds.)

Plasmas that encompass a range of temperatures and ionizations will produce weaker lines relative to the diffuse continuum because the metal lines form across limited column densities, while the diffuse continuum forms across the entire ionized (H II) zone. This situation occurs naturally in photoionized gas with a significant column. However, Figure 2 shows that the diffuse emission from the Ne VIII–emitting gas alone is again too weak to account for the BBB. In particular, the diffuse flux from the Ne VIII region is less than 10% of the incident BBB even for complete covering ($q = 1$), and the Ne VIII equivalent width measured relative to the diffuse continuum is ~330 Å, independent of the covering factor. Once again higher densities, in this case $\gtrsim 5 \times 10^{12}$ cm^{-3}, would be needed to adequenly weaken the lines via thermalization.

We conclude that the diffuse flux from the Ne VIII–emitting gas is signficantly weaker than the BBBs observed in AGNs if the densities are $\lesssim 5 \times 10^{11}$ cm^{-3}. The BBB must come from regions that are either ionized beyond Ne VIII or very dense and optically thick in the (metal) lines, so that their fluxes are greatly diminished relative to the continuum. Note that this conclusion also applies to the "very broad line region" that Ferland et al. (1990) identified with the broad, invariable components of Hα and Hβ in Mrk 590. Our results do not, contradict the Ferland et al. (1990) analysis, which shows that the measured broad Balmer components are consistent with (although somewhat weak for) the recombination fluxes they predict for optically thin gas capable of producing the BBB.

7. SUMMARY

Our main results are the following:

1. Ne VIII λ774 is the most likely identification for the strong, broad emission line near 774 Å (rest) in PG 1148+549 and other AGNs. The best alternatives to Ne VIII are N IV λ765 and O IV λ789; however, theoretical predictions for both photoionized and collisionally ionized plasmas, which encompass a wide range of physical conditions, show that these lines are weaker than Ne VIII in highly ionized gas and too weak compared to C IV λ1549 (and to the continuum in the photoionized case) at lower ionizations (§ 5). The measured line centroid in PG 1148+549 also favors the Ne VIII identification (§ 3).

2. If the gas is photoionized, our calculations with a standard ionizing spectrum indicate that the Ne VIII line forms in BELR components with high ionization parameters $5 \lesssim U \lesssim 30$ and temperatures 5×10^4 K $\lesssim T_e \lesssim 2 \times 10^5$ K, where the upper limits on U and T_e derive from the assumption of cloud stability. By comparison, typical estimates for the photoionized Lyα–C IV BELR indicate $U \lesssim 1$ and $T_e \lesssim 2 \times 10^4$ K.

3. The measured Ne VIII equivalent width requires total column densities $N_{\rm H} \gtrsim 10^{22}$ cm^{-2} and covering factors $q \gtrsim \frac{1}{3}$ (§ 6.1).

4. If the gas is collisionally ionized, equilibrium temperatures near 8×10^5 K would be needed for strong Ne VIII emission in thermally stable gas (§ 6.1).

5. In either case, the presence of broad Ne VIII λ774 implies that the BELR contains hotter and more highly ionized gas than previously recognized. This BELR component will appear as an X-ray warm absorber if it lies along our line of sight to the X-ray continuum source (§ 6.2).

6. Standard BELR space and column densities can lead to severe thermalization in some lines, such as C IV, but our photoionization calculations predict that Ne VIII is not affected for $n_H \lesssim 10^{11}$ cm^{-3}. The widely separated Ne VIII doublet should have a flux ratio of $\lambda 770/\lambda 780 \sim 2$ (§ 4.4).

7. The Ne VIII–emitting gas may have temperatures in the range needed for thermal-reprocessing models of the BBB, but for densities $\lesssim 5 \times 10^{12}$ cm^{-3} these regions produce too little diffuse continuum flux relative to the lines. The BBB must come from regions that are either ionized beyond Ne VIII or very dense and optically thick in the lines, so that their fluxes are greatly diminished relative to the continuum (§ 6.3).

Spectra at higher resolution and signal-to-noise ratios are needed to test the Ne VIII λ774 identification in PG 1148+549 and other QSOs. Simultaneous searches for Ne VIII and Mg X in the same spectra might provide the most reliable test of both identifications. Quality observations of AGN samples are also needed to study the amount and commonality of Ne VIII–emitting gas. Measurements of the Ne VIII doublet ratio would constrain the space and column densities (i.e., the product $n_e \tau_0$) in the Ne VIII region. Accurate line profiles and velocities would probe the relationship between Ne VIII and the rest of the BELR—for example, does Ne VIII λ774 continue the progression for larger blueshifts in higher ionization lines? Finally, the possible connection between the Ne VIII–emitting gas, the X-ray warm absorbers, and the associated Ne VIII line absorbers should be pursued. It is quite possible that these diverse observational features identify the same or related regions in a highly ionized component of the BELR (Shields 1994; Hamann et al. 1995a; § 6.2).

We are grateful to A. Kinney, K. Lanzetta, and D. Turnshek for kindly providing the *IUE* spectra for this study and to A. Diplas for help with the data processing. We also thank the referee, H. Netzer, for helpful comments and R. Antonucci, R. Cohen, V. Junkkarinen, and G. Kriss for useful discussions. This work was funded by NSF grant AST 93-19034 and by NASA grants NAG 5-1630, HR-1052.01-93A, AR-5292-93A, and LTSA NAGW-3315.

REFERENCES

Antonucci, R., & Barvainis, R. 1988, ApJ, 332, L13
Arnaud, M., & Rothenflug, R. 1985, A&AS, 60, 425
Baldwin, J. A., Ferland, G. J., Hamann, F., Carswell, R., Phillips, M., Wilkes, B., & Williams, R. E. 1995, in preparation
Barvainis, R. 1993, ApJ, 412, 513
Cochrane, D. M., & McWhirter, R. W. P. 1983, Phys. Scr., 28, 25
Cohen, R. C., et al. 1995, in preparation
Crenshaw, M. D., Bruegman, O. W., & Norman, D. J. 1990, PASP, 102, 463
Davidson, K., & Netzer, H. 1979, Rev. Mod. Phys., 51, 715
Della Ceca, R., Palumbo, G. G. C., Persic, M., Boldt, E. A., De Zotti, G., & Marshell, E. E. 1990, ApJS, 72, 471
Espey, B. R., Carswell, R. F., Bailey, J. A., Smith, M. G., & Ward, M. J. 1989, ApJ, 342, 666
Ferland, G. J. 1995, HAZY, a Brief Introduction to CLOUDY, internal report, Univ. Kentucky Dept. Phys. Astron.
Ferland, G. J., Korista, K. T., & Peterson, B. M. 1990, ApJ, 363, L21
Ferland, G. J., & Persson, S. E. 1989, ApJ, 347, 656
Ferland, G. J., Peterson, B. M., Horne, K., Welsch, W. F., & Nahar, S. N. 1992, ApJ, 387, 95
Ferland, G. J., & Rees, M. J. 1988, ApJ, 332, 141
Field, G. B. 1965, ApJ, 142, 431
Fiore, F., Elvis, M., Wilkes, B. J., & McDowell, J. 1993, ApJ, 415, 129
Frisch, H. 1984, in Methods in Radiative Transfer, ed. W. Kalkofen (Cambridge: Cambridge Univ. Press), 65
Gaetz, T. J., & Salpeter, E. E. 1983, ApJS, 52, 155
Gaskell, C. M. 1982, ApJ, 263, 79
Gehrels, N., & Williams, E. D. 1993, ApJ, 418, L25
George, I. M., Turner, T. J., & Netzer, H. 1995, ApJ, 438, L67
Grevesse, N., & Anders, E. 1989, in AIP Conf. Proc. 183, Cosmic Abundances of Matter, ed. C. I. Waddington (New York: AIP), 1
Halpern, J. P. 1984, ApJ, 281, 90
Hamann, F., Barlow, T. A., Beaver, E. A., Burbidge, E. M., Cohen, R. D., Junkkarinen, V., & Lyons, R. 1995a, ApJ, 443, 606
Hamann, F., & Ferland, G. J. 1992, ApJ, 391, L53
———. 1993, ApJ, 418, 11
Hamann, F., Zuo, L., & Tytler, D. 1995b, ApJ, 444, L69
Junkkarinen, V. T., et al. 1995, in preparation
Kaastra, J. S., Roos, N., & Mewe, R. 1995, A&A, 300, 25
Kallman, T. R., & Mushotzky, R. 1985, ApJ, 292, 49
Kellermann, K. I., Sramek, R., Schmidt, M., Shaffer, D. B., & Green, R. 1989, AJ, 98, 1195
Kinney, A. L., Bohlin, R. C., Blades, J. C., & York, D. G. 1991, ApJS, 75, 645
Koratkar, A. P., Kinney, A. L., & Bohlin, R. C. 1992, ApJ, 400, 435
Kriss, G. 1995, in The Analysis of Emission Lines, STScI Symp. Poster Papers, ed. M. Livio, 32
Krolik, J. H., & Kallman, T. R. 1984, ApJ, 286, 366
Krolik, J. H., McKee, C. F., & Tarter, C. B. 1981, ApJ, 249, 422
Kwan, J., & Krolik, J. 1981, ApJ, 250, 478
Lanzetta, K. M., Turnshek, D. A., & Sandoval, J. 1993, ApJS, 84, 109
Laor, A., & Netzer, H. 1989, MNRAS, 238, 897
Malkan, M., & Sargent, W. L. W. 1982, ApJ, 254, 22
Marshall, F. E., et al. 1993, ApJ, 405, 168
Mathews, W. G., & Ferland, G. J. 1987, ApJ, 323, 456
Mathur, S. 1994, ApJ, 431, L75
Mathur, S., Wilkes, B., Elvis, M., & Fiore, F. 1994, ApJ, 434, 493
Mendoza, C. 1983, in IAU Symp. 103, Planetary Nebulae, ed. D. R. Flower (Dordrecht: Reidel), 143
Morrison, R., & McCammon, D. 1983, ApJ, 270, 119
Nandra, K., & Pounds, K. A. 1994, MNRAS, 268, 405
Netzer, H. 1990, in Active Galactic Nuclei, ed. T. J-L. Courvoisier & M. Mayor (Berlin: Springer), 57
———. 1993, ApJ, 411, 594
Osterbrock, D. E. 1989, Astrophysics of Gaseous Nebulae and Active Galactic Nuclei (Mill Valley, CA: Univ. Sci. Press)
Peterson, B. M. 1993, PASP, 105, 1084
Rosenblatt, E. I., et al. 1995, in preparation
Sanders, D. B., Phinney, E. S., Neugebauer, G., Soifer, B. T., & Mathews, K. 1989, ApJ, 347, 29
Schmidt, M., & Green, R. 1983, ApJ, 269, 352
Shields, J. C. 1994, in Reverberation Mapping of the Broad-Line Region in AGNs, ed. P. Gondhalekar, K. Horne, & B. M. Peterson (ASP Conf. Ser. 69) (San Francisco: ASP), 293
Shields, J. C., & Ferland, G. J. 1993, ApJ, 402, 425
Shields, J. C., Ferland, G. J., & Peterson, B. M. 1995, ApJ, 441, 507
Shull, J. M., & Van Steenberg, M. 1982, ApJS, 48, 95
Stern, R., Wang, E., & Bowyer, S. 1978, ApJS, 37, 195
Timmes, F. X., Woosley, S. E., & Weaver, T. A. 1995, ApJS, 98, 617
Tytler, D., & Fan, X. M. 1992, ApJS, 79, 1
Wiese, W. L., Smith, M. W., & Glennon, B. M. 1966, Atomic Transition Probabilities (NBS-NSRDS 4, vol. 1) (Washington: GPO)